

# DENSITY FUNCTIONAL STUDY OF STRUCTURAL AND ELECTRONIC PROPERTIES OF Ca AND Mg DOPED TiO<sub>2</sub>

Mbae, J.K. and Muthui, Z.W.

Department of Physical Sciences, Chuka University, P. O. Box 109, 60400, Chuka  
Email: kathurejanem@gmail.com, ciku32ke@yahoo.com, zwanjiku@chuka.ac.ke

## ABSTRACT

The scarcity of affordable and environment-friendly sources of energy has led to emergence of photocatalysis to mitigate this problem. This is especially so if the photo catalysts are active in as much a wide region of the solar energy spectrum as possible. Environment-friendly, non-toxic and economical photocatalysts would find application in water treatment, providing another solution to the problem of clean water for domestic use. Of many materials available for photocatalysis is Titanium (IV) oxide (TiO<sub>2</sub>). It possesses many merits such as low cost, high photocatalytic activity, non-toxicity and high availability. However, drawbacks that limit its application include its optical absorption that falls in the ultraviolet part of the electromagnetic spectrum and rapid electron-hole recombination, which limits its photoquantum efficiency. To extend the optical absorption to a wider region of the solar energy spectrum, various dopants have been added to the oxide. In this study, the effect of doping rutile TiO<sub>2</sub> with alkaline earth metals Ca and Mg is investigated using the Density Functional Theory (DFT) method as implemented in the Quantum ESPRESSO simulation package, treating the exchange correlation potential with the Generalised Gradient Approximation. The optimized cell parameters for pure rutile crystal system are  $a = b = 4.603\text{\AA}$   $c = 2.992\text{\AA}$ , with a volume of  $63.393 (\text{\AA})^3$ . On doping there is a slight expansion of the crystal structure and its volume slightly increases by  $8.753 (\text{\AA})^3$  and  $28.816 (\text{\AA})^3$  with Mg and Ca doping respectively. The calculated band gap of undoped rutile is 1.8 eV. Mg and Ca doping raises the valence band edge by 0.2 eV in both Ca and Mg doped rutile. Dopant inter band and intra band states are observed that would be useful in mitigating against charge recombination hence enhancing the efficiency of the photocatalysts. Isolated O  $2p$  states are observed in the Projected Density of States (PDOS) of the doped systems which are normally attributed to enhanced optical absorption of photocatalysts in the visible region. Alkaline earth metal doping of TiO<sub>2</sub> rutile modifies the structural and electronic properties of rutile TiO<sub>2</sub> in a manner that would make it a more efficient photocatalyst. Co-doping with the alkaline metal dopants could be attempted to investigate the combined effect.

**Keywords:** Rutile TiO<sub>2</sub>, Density functional theory, Generalised gradient approximation, Doping, Band gap, Photocatalyst

## INTRODUCTION

Photocatalysis has emerged as one of the recent technologies for the mitigation against the scarcity, high prices and environmental pollution caused by fossil fuels in applications such as water treatment (Kang et al., 2019). Photodegradation using metal oxide photocatalysts is an efficient method for organic pollutant degradation and has proved to be an outstanding tool for degrading both aquatic and atmospheric organic pollutants. It uses the solar energy in the presence of a semiconductor photocatalyst to reduce the damage caused by environmental pollutants and wastewater treatment. Different semiconducting materials such as ZnO, CdS, ZnS, SnO<sub>2</sub>, WO<sub>3</sub>, Fe<sub>2</sub>O<sub>3</sub> and Nb<sub>2</sub>O<sub>4</sub> are abundantly available for photocatalysis, but only few of them are suitable for photo mineralization of a wide range of organic contaminants (Ahmed et al., 2013).

In the last three decades, Titanium (IV) Oxide (TiO<sub>2</sub>) photocatalysis has been one of the most promising environmental remediation technologies and an efficient technique for the treatment of contaminated

drinking and industrial wastewaters (Fujishima and Zhang, 2005; Tigabu *et al.*, 2021). The TiO<sub>2</sub> nanoparticle photocatalyst is capable of degradation and mineralization of many organic pollutants to harmless end products (Gaya and Abdullah, 2008). Moreover, TiO<sub>2</sub> photocatalyst also plays a key role in the redox reactions of heavy metals to insoluble state, with the subsequent recovery and removal from model industrial effluents (Avasarala et al., 2016). However, it suffers from a number of drawbacks that limit its application. First, its optical absorption falls in the ultraviolet part of the electromagnetic spectrum. To extend the optical absorption to a wider region of the solar energy spectrum, various dopants have been added to the oxide to improve its solar efficiency. TiO<sub>2</sub> has another major limitation of rapid electron-hole recombination which leads to low rates of the desired chemical transformations with respect to absorbed energy (Pesci *et al.*, 2013).

Various experimental and theoretical techniques such as metal and non-metal doping of TiO<sub>2</sub> have been undertaken in previous studies to make it more

technologically relevant and energy efficient (Graciani *et al.*, 2008). The use of non-toxic and readily available dopants to improve the application efficiency of TiO<sub>2</sub> has been a subject of both past and current research due to the wide applicability of the resulting materials in key areas such as water treatment and environmental remediation. Alkaline earth metal modified TiO<sub>2</sub> has been reported to demonstrate more efficient charge carrier separation from experimental approaches (Venkatachalam *et al.*, 2007; Li *et al.*, 2007; Zhang *et al.*, 2014; Lv *et al.* 2019; Rhatigan *et al.*, 2020). Mg doped TiO<sub>2</sub> has recently been reported to have improved degradation efficiency in both model industrial dyes (65–95%) and textile wastewater (92%) under natural sunlight (Shivaraju *et al.*, 2017).

The experimentally synthesized TiO<sub>2</sub> has been found to have a mixed phase composition, comprising mainly of the anatase and rutile phases. While the anatase phase has been found to be the more photoactive phase, the rutile phase has been found to be most thermodynamically stable (Kim *et al.*, 2021). More recently, theoretical approaches are proving complementary to the experimental efforts aimed at understanding and guiding the development of more

efficient photocatalysts. The anatase phase of TiO<sub>2</sub> in particular has been reported to cause a shift in absorption to longer wavelengths and improved optical absorbance in visible and near-IR region upon doping with alkaline earth metals and transition metal dopants (Ma *et al.*, 2015; Wang *et al.*, 2014). Due to the mixed phase composition of TiO<sub>2</sub>, a clear understanding on how each phase responds to modifications such as doping is pertinent in the development of more efficient photocatalysts. The anatase phase has dominated most of the theoretical investigations. This study focuses on modification of the structure and electronic properties of pure rutile TiO<sub>2</sub> by doping it with alkaline earth metals Ca and Mg, for improved photocatalytic applications.

## MATERIALS AND METHODS

Rutile TiO<sub>2</sub> has a tetragonal structure with space group 141/amd, having two titanium atoms and four oxygen atoms in the unit cell and experimental lattice parameters  $a = b = 4.57 \text{ \AA}$  and  $c = 2.95 \text{ \AA}$ . The crystal structure for computational model is as shown in Figure 1.

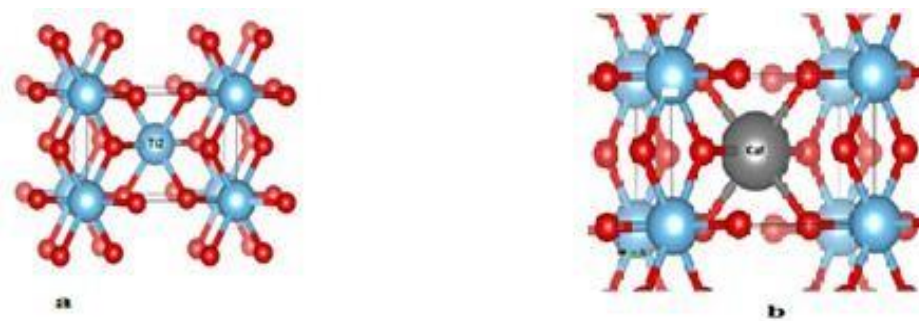


Figure 1: a) Rutile unit cell b) Rutile with doped element at Ti site

## Computational details

The Density Functional Theory (DFT) method as implemented by the Quantum ESPRESSO simulation package was used. The calculations to optimize the structure of rutile and to determine its electronic structure applied the Generalised Gradient Approximation (GGA) to describe the exchange and correlation in the system. In this work the electron wave functions were in plane wave basis sets with the cut off energy of the wave function converged at 40Ry. The ionic levels were represented by Ultrasoft Pseudopotentials (USPP) for Ti, O, Ca and Mg atoms. For total energy and relaxation calculations, a  $4 \times 4 \times 7$  k point grid was chosen using the linear tetrahedron

method with Blöchl corrections since it gives a smooth electron density of states. Electronic ground state energy was calculated through self-consistent cycles in combination with numerical methods such as David diagonalization schemes for evaluation of the solution to the Kohn Sham equation. Upon cation substitution, the structures were allowed to relax in order to minimize the forces in the system, before total energy calculations were done. The maximum number of geometric and electronic iterations was set at 100. The iterations ended at a convergence criterion of  $10^{-8}$  eV for most calculations. Generally, all calculations began from scratch.

## RESULTS AND DISCUSSION

### Structural Properties

The optimized cell parameters for pure rutile TiO<sub>2</sub> are  $a = b = 4.603 \text{ \AA}$ ,  $c = 2.992 \text{ \AA}$ , which are in good agreement with other theoretical values such as  $a = b = 4.614 \text{ \AA}$ ,  $c = 2.976 \text{ \AA}$  (Liu et al., 2010) and others in Table 1. The cell parameters calculated from this work using GGA are very close to experimental values, showing the reliability of the method. To analyze geometrical changes after the dopant entering the

lattice, the optimized cell parameters were calculated for the different doped models, as shown in Figure 2. In comparison to pure rutile TiO<sub>2</sub>, the doped systems have larger lattice parameters, with the Ca-doped system being the largest. This is attributed to its larger ionic radius compared to Mg and Ti. On doping there is a slight expansion of the crystal structure and its volume slightly increases by 8.753 (Å)<sup>3</sup> and 28.816 (Å)<sup>3</sup> in Mg and Ca doped systems respectively.

**Table 1: Cell parameters and crystal volume changes for the pure and doped rutile TiO<sub>2</sub>**

| Configuration             | a (Å)                                 | b(Å)               | c(Å)               | V(Å) <sup>3</sup> | ΔV(Å) <sup>3</sup> |
|---------------------------|---------------------------------------|--------------------|--------------------|-------------------|--------------------|
| Pure Rutile               | 4.603                                 | 4.603              | 2.992              | 63.393            | -                  |
| Other theoretical results | 4.602 <sup>1</sup>                    | 4.602 <sup>1</sup> | 2.977 <sup>1</sup> |                   |                    |
|                           | 4.630 <sup>2</sup>                    | 4.630 <sup>2</sup> | 2.980 <sup>2</sup> |                   |                    |
|                           | 4.593 <sup>3</sup>                    | 4.593 <sup>3</sup> | 2.940 <sup>3</sup> |                   |                    |
|                           | 4.623 <sup>4</sup> 4.459 <sup>5</sup> | 4.623 <sup>4</sup> | 2.987 <sup>4</sup> |                   |                    |
|                           | 4.690 <sup>6</sup>                    | 4.459 <sup>5</sup> | 2.902 <sup>5</sup> |                   |                    |
|                           | 4.594 <sup>7</sup>                    | 4.690 <sup>6</sup> | 2.990 <sup>6</sup> |                   |                    |
|                           | 4.594 <sup>7</sup>                    | 4.594 <sup>7</sup> | 2.959 <sup>7</sup> |                   |                    |
| Experimental results      | 4.587 <sup>1</sup> 4.593 <sup>2</sup> | 4.587 <sup>1</sup> | 2.955 <sup>1</sup> |                   |                    |
|                           |                                       | 4.593 <sup>2</sup> | 2.959 <sup>2</sup> |                   |                    |
|                           |                                       |                    |                    |                   |                    |
| Mg doped Rutile           | 4.736                                 | 4.736              | 3.221              | 72.246            | 8.753              |
| Ca doped Rutile           | 4.974                                 | 4.974              | 3.73               | 92.209            | 28.816             |

<sup>1</sup>(Rubio-Ponce et al., 2008) <sup>2</sup>(Burdett et al., 1987) <sup>3</sup>(Chen et al., 2018) <sup>4</sup>(Muscat et al., 1999) <sup>5</sup>(Liu et al., 2009) <sup>6</sup>(Lindan et al., 1997) <sup>7</sup>(Zeng, 2015)

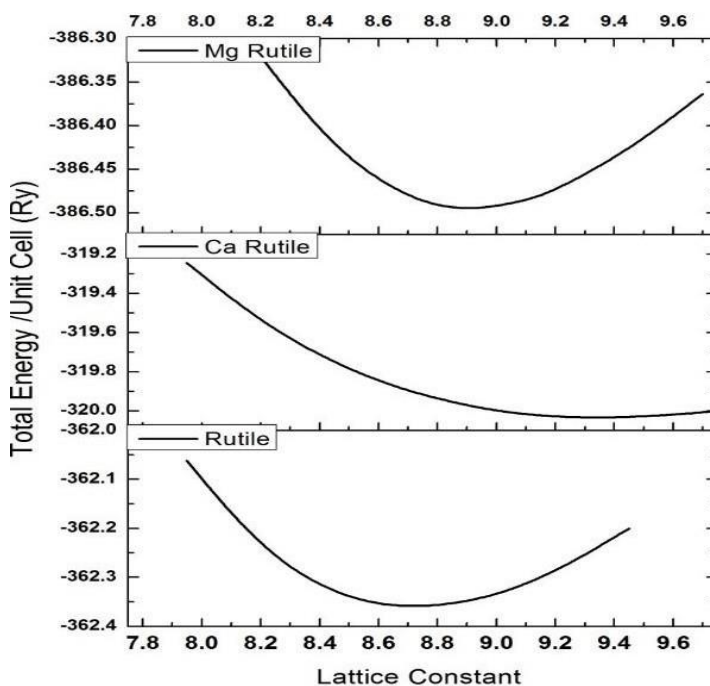


**Figure 2: Total energy vs lattice constants of pure and doped rutile**

## ELECTRONIC PROPERTIES

### Total Density of States (TDOS) and Projected Density of States (PDOS)

Figure 3 shows the TDOS and the PDOS for pure rutile TiO<sub>2</sub>. The valence band of pure rutile is mainly composed of the O *p* orbitals, while the conduction band is mainly comprised of the Ti *d* orbital. PDOS shows a shifting of the valence band edge to higher energy in the doped systems. This is mainly due to the introduction of dopant states within the energy region as shown in Figure 4, which contributes to

hybridization with the O *2p*, Ti *3d* states of rutile. Similarly, Ca dopant states are found at the valence band edge, leading to the formation of interband states and a shifting of the valence band to higher energies as shown in Figure 5, an effect favorable for the enhancement of photocatalysis.

Investigation of the charge density difference reveals a change in the shape of charge distribution around the oxygen atoms for the different systems even at this very low dopant concentrations as shown in Figure 6.

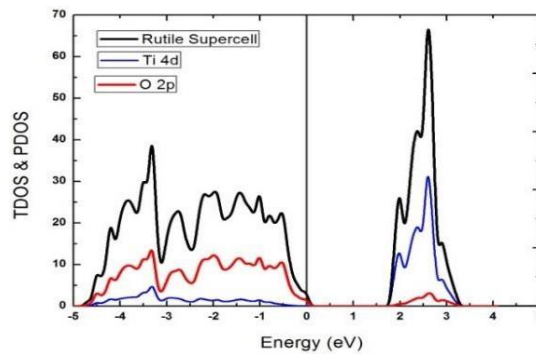


Figure 3: TDOS and PDOS of pure Rutile

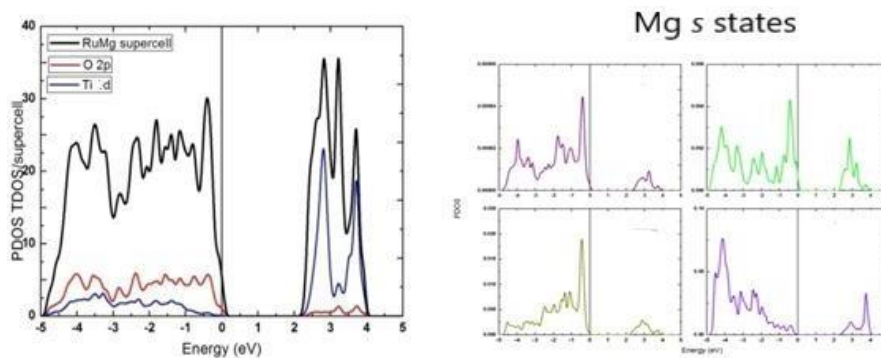


Figure 4: TDOS and PDOS Mg doped Rutile

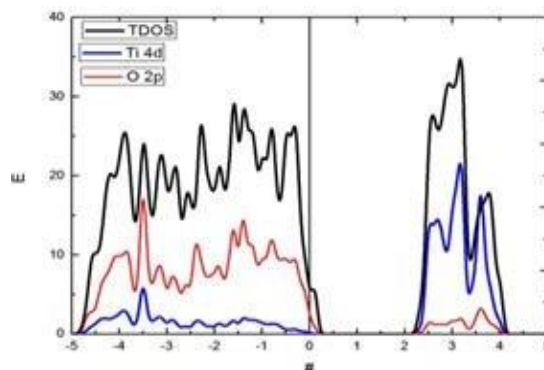


Figure 5: TDOS and PDOS of Ca doped Rutile

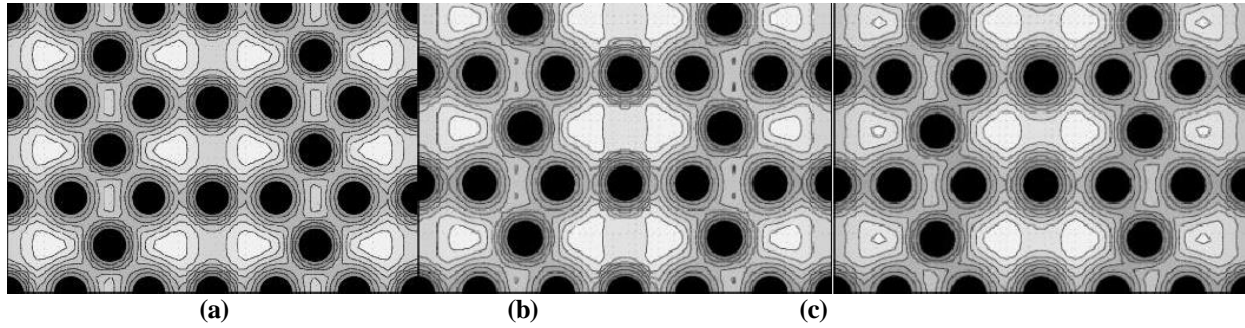


Figure 6: Charge density maps of (a) rutile, (b) Mg and (c) Ca doped rutile

### Band structures

The pure rutile TiO<sub>2</sub> band structure is shown in Figure 7. The Fermi level has been chosen at zero-point energy, which is shown as the dotted line in the figure. The calculated band gap of pure rutile is 1.8 eV which

agrees well with the band gap from other theoretical calculations such as 1.86 eV calculated by Jin feng et al., 2014 as well as results from other studies. Table 2 is a comparison of the findings with previous theoretical and experimental studies.

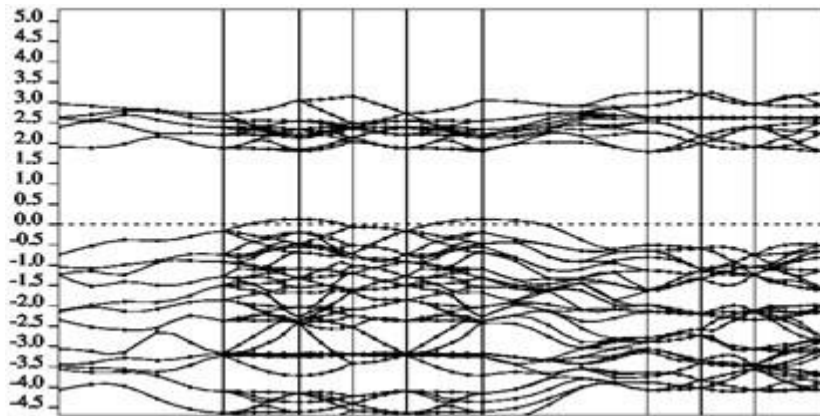


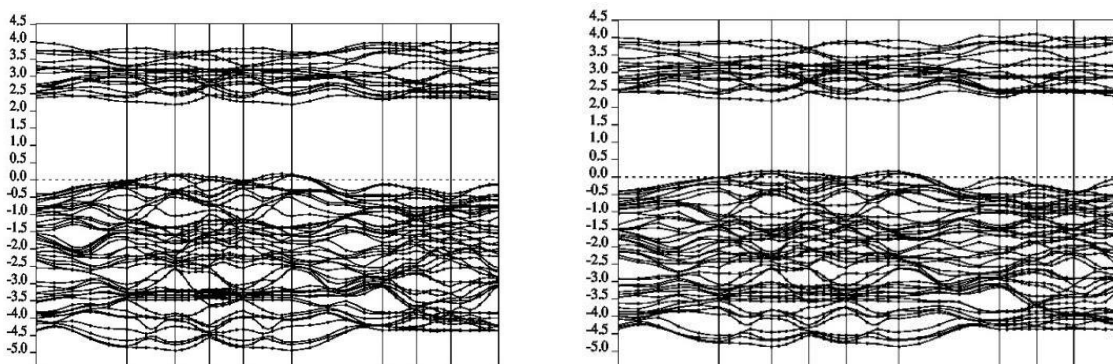
Figure 7: Band structure of pure rutile.

Table 2: Rutile band gap and other theoretical and experimental results

| Rutile TiO <sub>2</sub>   | Band gap (eV)                |
|---------------------------|------------------------------|
| This work                 | 1.80                         |
| Other theoretical results | 1.86 (Jin feng et al.,2014)  |
|                           | 1.87 (Chen et al.,2017)      |
|                           | 1.90 (Lindan et al., 1997)   |
|                           | 1.78 (Shang and Ching, 1995) |
|                           | 2.10(Guo et al., 2011)       |
| Experimental results      | 2.05 (Zeng et al., 2015)     |
|                           | 3.00 (Pascual et al., 1978)  |
|                           | 3.00 (Landmann et al., 2012) |
|                           | 3.00 (Reyes et al., 2008)    |

The calculated values are however less than the experimental value of 3.0 eV. This is expected since DFT underestimates the band gaps of insulators and semiconductors, but provides the necessary qualitative understanding of the effect of defects introduced on the trend in the change of the band gap upon introduction of defects.

Ca and Mg dopants generate dopant states in the band gap, near the top of valence bands hence shifting valence bands to higher energy region, with a corresponding reduction in the band gap, even at this very low doping concentrations. The states are about 0.2 eV above the Fermi level for both Mg doped and Ca doped rutile as shown in Figure 8.



**Figure 8: Band structure for Mg and Ca doped Rutile**

## CONCLUSION

There is a shift of the valence band edge towards higher energies and introduction of intraband dopant states with a corresponding reduction in the band gap. The observed changes in the electronic structure are favorable for the absorbance of a wider spectrum of solar energy and reduction of charge recombination during photocatalysis. Alkaline earth metal doping of TiO<sub>2</sub> rutile modifies the structural and electronic properties of rutile TiO<sub>2</sub> in a manner that would make it a more efficient photocatalyst

## RECOMMENDATIONS

Co-doping with the alkaline metal dopants could be attempted to investigate the combined effect.

## ACKNOWLEDGEMENT

The authors are grateful to the Centre for High Performance Computing (CHPC) in South Africa for giving us the platform to carry out this research.

## REFERENCES

- Ahmed, A., Abdi, E., Mahmmoud, S., Abdi, S., Mohamed, M., El-Sayed, B. and Fawzy, H. 2013. Characterization and Photocatalytic Efficiency of Palladium Doped-TiO<sub>2</sub> Nanoparticles. *Advances in Nanoparticles*, 2(4):24051.
- Avasarala, B., Tirukkovalluri, S. and Bojja, S. 2016. Magnesium Doped Titania for Photocatalytic

- Degradation of Dyes in Visible Light. *Journal of Environmental and Toxicology*, 6(2):358.
- Burdett, J.K., Hughbanks, T., Miller, G.J., Richardson, J.W. and Smith, J.V. 1987. Structural-electronic relationships in inorganic solids: Powder neutron diffraction studies of the rutile and anatase polymorphs of titanium dioxide at 15 and 295 K. *Journal of the American Chemical Society*, 109(12):3639–3646.
- Chen, H., Li, X., Wan, R., Kao-Walter, S. and Lei, Y. 2018. A DFT study of the electronic structures and optical properties of (Cr, C) co-doped rutile TiO<sub>2</sub>. *Chemical Physics*, 501:60–67.
- Gaya, U.I. and Abdullah, A.H. 2008. Heterogeneous photocatalytic degradation of organic contaminants over titanium dioxide: A review of fundamentals, progress and problems. *Journal of Photochemistry and Photobiology C: Photochemistry Reviews*, 9(1):1–12.
- Graciani, J., Álvarez, L.J., Rodriguez, J.A. and Sanz, J. Fdez. 2008. N Doping of Rutile TiO<sub>2</sub> (110) Surface. A Theoretical DFT Study. *The Journal of Physical Chemistry C*, 112(7):2624–2631.
- Guo, Y., Lu, X., Zhang, H., Weng, J., Watari, F. and Leng, Y. 2011. DFT Study of the Adsorption of the Aspartic Acid on Pure N-Doped and Ca-Doped Rutile (110) Surfaces. *The Journal of Physical Chemistry C*, 115(38):18572–18581.
- Fujishima, A. and Zhang, X. 2005. Titanium Dioxide Photocatalysis: Present Situation and Future

- Approches. *Comptes Rendus Chimie*, 9(5-6):750–760.
- Kang, X., Liu, S., Dai, Z., He, Y., Song, X. and Tan, Z. 2019. Titanium Dioxide: From Engineering to Applications. *Catalysts*, 9(2):191.
- Kim, M. G., Kang, J. M., Lee, J. E., Kim, K. S., Kim, K. H., Cho, M. and Lee, S. G. 2021. Effects of Calcination Temperature on the Phase Composition, Photocatalytic Degradation, and Virucidal Activities of TiO<sub>2</sub> Nanoparticles. *ACS Omega*, 6(16):10668–10678.
- Landmann, M., Rauls, E. and Schmidt, W. 2012. The Electronic Structure and Optical Response of Rutile, Anatase and Brookite TiO<sub>2</sub>. *Journal of physics; condensed matter*, 24:195503.
- Li, Y., Peng, S., Jiang, F., Lu, G. and Li, S. 2007. Effect of doping TiO<sub>2</sub> with alkaline-earth metal ions on its photocatalytic activity. *Journal of Serbian Chemical Society*, 72(4):393–402.
- Lindan, P.J.D., Harrison, N. M., Gillan, M. J. and White, J.A. 1997. First-principles spin-polarized calculations on the reduced and reconstructed TiO<sub>2</sub> (110) surface. *Phys. Rev. B*, 55(23):15919–15927.
- Liu, H., Liu, G. and Zhou, Q. 2009. Preparation and characterization of Zr doped TiO<sub>2</sub> nanotube arrays on the titanium sheet and their enhanced photocatalytic activity. *Journal of Solid State Chemistry*, 182(12): 3238–3242.
- Ma, J.-G., Zhang, C.-R., Gong, J.-J., Wu, Y.-Z., Kou, S.-Z., Yang, H., Chen, Y.-H., Liu, Z.-J. and Chen, H.-S. 2015. The Electronic Structures and Optical Properties of Alkaline-Earth Metals Doped Anatase TiO<sub>2</sub>: A Comparative Study of Screened Hybrid Functional and Generalized Gradient Approximation. *Materials (Basel, Switzerland)*, 8(8):5508–5525.
- Muscat, J., Harrison, N.M. and Thornton, G. 1999. Effects of exchange, correlation, and numerical approximations on the computed properties of the rutile TiO<sub>2</sub> (100) surface. *Phys Rev B*, 59(3):2320–2326.
- Pascual, J., Camassel, J. and Mathieu, H. 1978. Fine structure in the intrinsic absorption edge of TiO<sub>2</sub>. *Phys. Rev. B.*, 18(10):5606.
- Pesci, F.M., Wang, G., Klug, D. R., Li, Y. and Cowan, A. J. 2013. Efficient Suppression of Electron-Hole Recombination in Oxygen-Deficient Hydrogen-Treated TiO<sub>2</sub> Nanowires for Photoelectrochemical Water Splitting. *The Journal of Physical Chemistry. C, Nanomaterials and Interfaces*, 117(48):25837–25844.
- Reyes, C., Rodríguez, G., Espinosa, P., Cab, C., Coss, R. and Oskam, G. 2008. Phase-pure TiO<sub>2</sub> nanoparticles: anatase, brookite and rutile. *Nanotechnology* 19: 145605.
- Rhatigan, S., Sokalu, E., Nolan, M. and Colón, G. 2020. Surface Modification of Rutile TiO<sub>2</sub> with Alkaline-Earth Oxide Nanoclusters for Enhanced Oxygen Evolution. *ACS Applied Nano Materials*, 3(6):6017-6033.
- Rubio-Ponce, A., Conde-Gallardo, A. and Olgún, D. 2008. First-principles study of anatase and rutile TiO<sub>2</sub> doped with Eu ions: A comparison of GGA and LDA+U calculations. *Phys. Rev. B*, 78(3):035107.
- Shang, D. and Ching, W. 1995. Electronic and optical properties of three phases of titanium dioxide: Rutile, anatase, and Brookite. *Physical Review B*, 51(19):13023.
- Shivaraju, H.P., Midhun, G., Anil Kumar, K.M., Pallavi, S., Pallavi, N. and Behzad, S. 2017. Degradation of selected industrial dyes using Mg-doped TiO<sub>2</sub> polyscales under natural sun light as an alternative driving energy. *Applied Water Science*, 7(7):3937–3948.
- Tigabu, B. M., Abi, T. M. and Hirpo H. D. 2021. Photocatalytic Degradation of Organic Pollutants: The Case of Conductive Polymer Supported Titanium Dioxide (TiO<sub>2</sub>) Nanoparticles: A Review. *Nanoscience and Nanometrology*, 7(1):1-13.
- Venkatachalam, N., Palanichamy, M., Arabindoo, B. and Murugesan, V. 2007. Alkaline earth metal doped nanoporous TiO<sub>2</sub> for enhanced photocatalytic mineralisation of bisphenol-A. *Catalysis Communications*, 8(7):1088–1093.
- Wang, Y., Zhang, R., Li, J., Li, L. and Lin, S. 2014. First-principles study on transition metal-doped anatase TiO<sub>2</sub>. *Nanoscale Research Letters*, 9(1):46.
- Zeng, Z.-L. 2015. First-Principles Study on the Structural and Electronic Properties of N Atoms Doped-Rutile TiO<sub>2</sub> of Oxygen Vacancies. *Advances in Materials Science and Engineering*, 2015(670243):1-10.
- Zhang, J., Qian, L., Fu, W., Xi, J., and Ji, Z. 2014. Alkaline-Earth Metal Ca and N Codoped TiO<sub>2</sub> with Exposed 001 Facets for Enhancing Visible Light Photocatalytic Activity. *Journal of the American Ceramic Society*, 97(8):2615–2622.